Shape Morphing as a Minimal Path in the Graph of Cubified Shapes

Raphaël Groscot and Laurent D. Cohen

University Paris-Dauphine, PSL Research University, CEREMADE, CNRS UMR 7534, 75016 Paris, France

Abstract: The systematic study of morphings for non parametric shapes suffers from ambiguities in defining good general morphings, such as the trade-off between plausibility and smoothness, above all under large topology changes. In the recent years, only neural networks have offered a generic solution, using their latent space as a shape prior. But these models are optimized for single shape reconstruction, giving little control on the generated morphings. In this paper, we show how qualitatively similar results can be achieved when replacing neural networks with a set of carefully crafted components: a style-content separation method via the fitting of a Deformable Voxel Grid, a similarity metric adapted to the extracted content, and a formulation of morphings as minimal paths in a graph. While forgoing the automatic learning of a generative model, we still achieve similar morphing capabilities. We performed various evaluations, quantitative analysis on the robustness of our proposed method and on the quality of the results, and demonstrate the usefulness of each component. Finally, we provide guidance on how manual intervention can improve quality. This is indeed possible since, unlike neural networks, each component in our method is interpretable.

1 INTRODUCTION

In the literature, the study of shape morphings typically follows one of two assumptions: (a) both shapes have a shared connectivity, generally because they embody the same type of shape (e.g. human or animal bodies), and the goal is to find a plausible movement between two configurations; or (b) the two shapes are considered in a vacuum, without external shape priors, and the goal is to find a deformation from one to the other, which minimizes a certain distortion criteria (e.g. for pairs of arbitrary shapes).

Given the creative opportunities of morphing for computer graphics, it is desirable to develop methods with a wider applicability. In the recent years, generative neural networks such as auto encoders and GANs have not only proven powerful to generate realistic 3D shapes, in various formats (voxels, pointclouds, or meshes), but also offer a latent space amenable to shape interpolations. By design, this learned representation provides a shape prior, constraining generated shapes to be similar to the training set. However, they are generally not built nor trained towards the end of producing meaningful morphings. Rather, their morphing capabilities appear as a mere byproduct of latent space interpolation. Most works relying on them focus their efforts on the quality and expressivity of the outputs, as they are generally mainly evaluated on the reconstruction of known shapes.

These generative models benefit from their ability to learn, without supervision, an invertible encoding which brings similar shapes close together. We explore the possibility of achieving similar results with traditional, explicit methods. Doing so, we simultaneously address the typical limitations of deep learning; namely, the lack of interpretability, and the need for expensive and powerful hardware capable of parallel computing.

As a matter of fact, the present work stems from the intuition that medium-sized datasets contain enough shapes to express novel shapes as simple combinations and deformations of the existing ones. As a result, we seek to generate "good" morphings whose intermediate states are existing shapes, up to a small deformation. Moreover, we do not want to rely on any class-specific parameterization.

To this end, we propose three interconnected components:

1. a class-independent shape descriptor, relying on a particular case of style and content separation, which we named "cubifiction";

2. a deformation metric compatible with this content descriptor;

3. a graph-based framework for finding minimal-energy shape morphings.

The first and second steps respectively provide nodes and links to ultimately build a shape graph. It can be seen as a discretized version of a latent space, where the intermediate representation is not learned but handcrafted in accordance with the strong symmetries found in certain shapes, such as chairs or tables. As a matter of fact, our content descriptor derives from a cubification of the shapes, which appears to consistently locate the semantic parts of different shapes.

This is performed via the optimization of a Deformable Voxel Grid (DVG), presented in Section 3. Then, Section 4 explains the construction of a graph shape-space which encapsulates the similarities in terms of shape content. We then present experimental results and evaluations in Section 5. Finally, Section 6 provides an extensive analysis of many design elements of our method, discussing the influence and interactions of its different components.

2 RELATED WORK

Deep Learning and Shape Latent Spaces

In this area, use cases typically include one of the following tasks: shape processing and data augmentation (Park et al., 2017; Fish et al., 2014; Kalogerakis et al., 2012; Haibin et al., 2015; Li et al., 2017), shape prediction from 2D data (Shin et al., 2018; Haibin et al., 2015; Wu et al., 2016; Wang et al., 2018; Fan et al., 2016), shape completion (Allen et al., 2003; Groueix et al., 2018; Park et al., 2019), and latent space exploration (Tulsiani et al., 2017; Wu et al., 2016; Li et al., 2017; Achlioptas et al., 2017; Groscot et al., 2019; Dubrovina et al., 2019).

Over the past years, generative models, using architectures inspired by Variational Auto Encoders (Kingma and Welling, 2013) and GANs (Goodfellow et al., 2014), have been used for shape morphing, via linear interpolations in the latent space. Works can represent shapes in various formats, such as point-clouds (Qi et al., 2016; Qi et al., 2017; Fan et al., 2016; Achlioptas et al., 2017; Groscot et al., 2019), voxels (Wu et al., 2016; Li et al., 2017; Dubrovina et al., 2019), octrees (Tatarchenko et al., 2017), or 4D particle dynamics (Niemeyer et al., 2019).

Other works, focusing on the prediction of a 3D shape from a given image, used more specific representations such as surface patches (Groueix et al., 2018) or deformed ellipsoids (Wang et al., 2018), but they do not appear to offer a direct way of producing shape morphings. More recently, networks predicting implicit functions (Park et al., 2019; Hao et al., 2020) appeared to allow smooth, arbitrary-topology meshes, while being compatible with latent space interpolations.

Deep learning approaches are based on the assumption that learned descriptors, as opposed to handcrafted ones, are better suited to capture the variability of natural signals. Moreover, generative models offer a latent space amenable to the generation of new shapes. However, neural networks come with known limitations: their lack of interpretability and their constraints to converge to visually-pleasing results. As a matter of fact, they typically require rich databases, powerful GPUs, and suffer from long training times and difficult parameters tuning. All this makes reproducing the results of deep learning based methods hard, even when a portion of the code is public.

Our work takes quite an opposite view, exploring the possibility of achieving similar results without any neural network. We show in fact that we can obtain the same capabilities offered by generative networks' latent spaces, by carefully handcrafting and designing every component. As a result, we already generate satisfying results even with modest datasets (around 500 shapes), and because every component has a clear meaning, one can easily improve the desired outcome by manual intervention.

In a way, this work ultimately consists in investigating what remains once those applications are stripped from neural networks, in order to better understand the specificities they bring.

Morphing Based on Deformations

The problem of realistic shape morphing was tackled by (Gao et al., 2013) for human and animal bodies, interpreting a collection of shapes as a deformation space. By establishing shape correspondences, they obtain a shape distance allowing them to express morphings as a minimal path among clusters of similar body poses. We adopt a framework similar to theirs, while focusing on shapes which have varied topologies and no natural parameterization, such as chairs and sofas, such that a morphing cannot be interpreted as a mere deformation. Our work can be seen as a derivation of the same ideas, but adapted to different modalities, typically addressed by deep learning methods.

As far as they are concerned, instead of relying on geometric generative models, shape deformation is another popular choice to generate realistic shapes at a small cost, leveraging the similarity between objects belonging to the same class. To parameterize these deformations, most approaches (Hanocka et al., 2018; Kurenkov et al., 2017) use the Free Form Defor-

mation (Sederberg and Parry, 1986), which arranges control points on a regular volumetric grid, and then uses cubic interpolation to distort the object as the points move. The key differences with our model are the following. First, they tackle different problems, such as partial shape alignment (Hanocka et al., 2018) or shape reconstruction by deforming a template (Kurenkov et al., 2017). Second, and most importantly, their shape deformations are pair-specific, trained to predict deformations between pairs $((A,B)$ where A is deformed into B). On the contrary, our model provides a consistent shape cubifiction, without any learning, allowing to compare all shapes (in terms of similarity measure); and we use this representation to estimate minimal-energy morphings.

More recently, (Zheng et al., 2020) showed how to reconstruct shapes by deforming an implicit template, predicted by a neural network, giving shape correspondences and deformations. In our method, we can see the cubifiction step as a template deformation, where the template is the unit cube, and where the deformation is not learned but computed. We try to achieve similar results, in surface quality and interpolation smoothness, but without the constraints and limitations of deep learning as explained above.

Parametric and Statistical Shapes Descriptors

Describing a shape class by a given set of parameters (also referred to as a *dictionary*) is a fundamental operation for applications such as classification, model retrieval, or similarity search. Some approaches (Kalogerakis et al., 2012; Haibin et al., 2015) learn probabilistic distributions of shapes from the properties of their semantical parts, or even from the relations between parts simplified into simpler geometric primitives (Tulsiani et al., 2017). Others learn explicit parameterizations, typically possible on shapes representing body poses (Allen et al., 2003).

Our method relies on shape cubifiction, serving as a shape descriptor which, while being class-independent, is more adapted to shapes having strong reflection symmetries. The key difference with these other methods is twofold. First, we show how traversing the space of plausible shapes does not require statistical inference but can be expressed as a minimal-path problem in a graph, whose structure captures the geometric relations between existing shapes. Second, our descriptor is invertible, which allows us to generate new shapes (for the intermediate states of morphings), without any neural network.
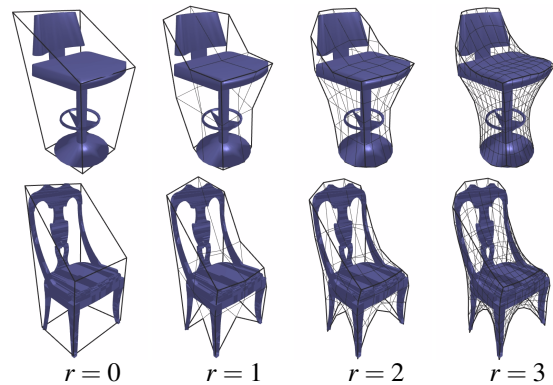

Figure 1: Optimization of DVGs at progressive resolutions r (constant number of steps per r).

Deformable Voxel Grids

Our cubifiction relies on Deformable Voxel Grids (Groscot, 2021; Groscot and Cohen, 2022), a model inspired by the Topological Active Volume (TAV) from (Barreira et al., 2003), which is a volumetric extension of active contours (Kass et al., 1988; Cohen, 1991). The unfamiliar reader can think of active contours as parametric curves which minimize a given energy, typically used for segmenting objects in images (Hemalatha et al., 2018). In the case of DVGs, the energy ensures that after an initialization as a regular voxel grid around the input shape, the grid is optimized until it tightly and smoothly embraces the shape (see Figure 1).

3 INVERTIBLE CUBIFICTION VIA DVGs

The purpose of cubifiction is to offer a consistent representation basis for several shapes belonging to the same class (e.g. chair or car): the same semantical parts of different objects tend to occupy the same region of the cube, allowing for easier shape comparisons (see how we define a distance between cubified shapes in Section 4). In order to do so, we optimize a DVG and interpret it as a smooth deformation of the unit cube $\mathbb{R}^3$ adapted to a given shape S, and apply the inverse deformation to S.

3.1 Forward DVG Projection

For a given DVG cell c, a point q inside can be expressed by its *local coordinates*, a triplet in $[0,1]^3$:

$$\tilde{u}, \tilde{v}, \tilde{w} \in [0,1]^3 \text{ s.t. } f_c(\tilde{u}, \tilde{v}, \tilde{w}) = q \qquad (1)$$

where $p_1, p_2, \ldots, p_8$ are the positions of the eight

(a) Bilinear interpolation

(b) DVG-voxel correspondence

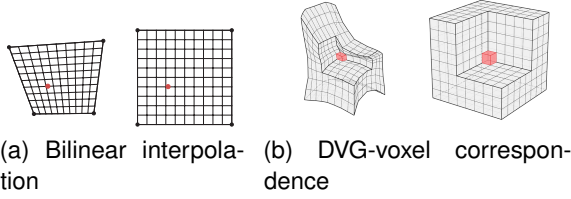Figure 2: A natural way of setting grid coordinates on a quadrilateral is via bilinear interpolation, which maps regular subdivisons of $[0,1]^2$ onto the quad cell (*left to right*). Determining the local coordinates of a given point within the cell corresponds to inverting this interpolation (*right to left*). The same is done for registering a point inside a DVG, but in 3D, with the inversion of a trilinear interpolation.

vertices of c. The interpolator f_c can be linear or smooth (we use, respectively, a trilinear p^V_{tri} and a Thin Plate Spline p^V_{tps} interpolators). Both can be defined by matching the control points V^0 of a regular cube to V, those of a given DVG.

Then, an affine transformation maps the cell to its correct location within the whole DVG grid system (see Figure 2).

3.2 Backward DVG Projection

We suppose the signed distance field (SDF) of shape S is given. Each cell of V is subdivided into smaller subcells, and the value of the SDF is queried at the locations of each subcell centroid, which naturally have (u,v,w) coordinates, coming from the indexing of V: vertex index (i,j,k) has local coordinates $(u,v,w) = (\frac{i}{r-1}, \frac{j}{r-1}, \frac{k}{r-1})$. The cubified SDF can be used in two ways.

Shape Cubifiction and Reconstruction: Using marching cubes (Lorensen and Cline, 1987), we obtain C, the mesh of the cubified shape, where the precision of the geometry is limited by the grid resolution of the DVG and the number of cell subdivisions. The original shape can be recovered by projecting C into V using the spline projector p^V_{tps}. This operation is important because it gives the baseline shape representation capacity for the morphings we generate: as a matter of fact, our morphings are done in V-space and C-space separately, and use the p^V_{tps} projector to effectively create the intermediate shapes. The intuition is that the DVG separates style and configuration, respectively into C and V. This way, we find morphings that minimize the amount of displaced mass to transfer style (C), while the deformation abilities of the grid allow to interpolate the configurations V.

Figure 4 shows examples of such cubifictions and reconstructions using both p^V_{tri} and p^V_{tps}.

Content Descriptor: We can extract the volume indicator function $\mathbb{1}_S$ by thresholding the SDF. Its average value is binned within each DVG cell, in order to obtain an r^3 voxel image which serves as a shape content descriptor. Each cell value, between 0 and 1, represents the proportion of the cell which intersects the shape. This descriptor allows to regroup models by similarity in order to build a shape graph, as explained in the following Section.

4 GRAPH-BASED SHAPE SPACE

After all shapes of a dataset are consistently cubified, we propose to discretize the global shape space in the form of a weighted graph, whose edges derive from a similarity measure between cubified shapes. This graph formalizes the notion of shape morphing, as a morphing from shape A to B will correspond to a minimal path from node $\mathcal{N}_A$ to $\mathcal{N}_B$. This choice is motivated by the fact that for a large enough shape dataset, most intermediate steps of a morphing are close to existing shapes.

This is why we explore the possibility of discrete morphings, restricted to known shapes, effectively bypassing the necessity to learn how to sample new shapes; while imposing them a minimal energy criteria.

We first present a general framework for shape morphings as minimal paths in a shape graph, for any arbitrary shape embedding. Then, we show how it can be used with cubified shapes and how our invertible cubifiction actually allows to easily extrapolate the discrete morphings to continuous ones.

4.1 Morphings as Minimal Paths

In this part, we consider the problem of morphings with shape priors, that is to say, morphings such that intermediate states are plausible. We operate under the minimal assumption that the shape prior is given by a finite set of exemplars, $\mathcal{S} = \{S_1, \cdots, S_N\}$, where the shapes are given in an arbitrary embedding. A morphing corresponds to a sequence of shapes from $\mathcal{S}$, but we want a metric to evaluate the quality of a morphing. In order to do so, we impose a cost (or an energy) to a morphing:

$$E(M = (S_1, \cdots, S_k)) \triangleq \sum_{i=1}^{k-1} E(S_i, S_{i+1}) \qquad (2)$$

Where $E(S_i, S_j)$ is the energy of the transition $S_i \to S_j$. Such energies can be evaluated as paths length in a weighted graph $\mathcal{G}$ defined by:

- nodes $\{\mathcal{N}_1, \cdots, \mathcal{N}_N\}$, corresponding to the shapes in $\mathcal{S}$;

- positive weighted edges $\{w_{i,j}\}$ where w_{ij} can be interpreted as a similarity between shapes S_i and S_j. By convention, an absent edge (i, j) is equivalent to $w_{ij} = \infty$.

We call a morphing $A \to B$ *minimal* if it is achieved by a shortest path in $\mathcal{G}$ from $\mathcal{N}_A$ to $\mathcal{N}_B$. In order to consider symmetric morphings (i.e. equal to the time-reversed morphing), we assume $\mathcal{G}$ in an undirected graph, i.e, $\forall i, j, w_{i,j} = w_{j,i}$.

4.2 Graph of Cubified Shapes

We can apply the previous formalism to the space of cubified shapes. We propose a metric between shapes cubified via a DVG (according to the method described in Section 3), which interprets as an approximate transport cost.

We first compute the volumetric DVG descriptor (see 3.2), where each cell of the DVG is attributed a value between 0 and 1, corresponding to the proportion of the cell which is occupied by the shape. This provides a voxel image of a cubified shape. With a DVG resolution $r = 8$, this leads to a representation space with $8^3 = 512$ dimensions, enough for the curse of dimensionality to prevent Euclidian distances from being meaningful. This naive approach does not leverage the proximity of the cells, which is why we propose a method based on the morphological dilation operator.

Atypical Models Detection and Removal

A preliminary step is to exclude models for which the aforementioned volumetric descriptor is inadequate, that is to say, when the density of presence inside the cells is not homogeneous. To detect such models, we simply compute and sum all the inner-cell standard deviations of the discrete $\mathbb{1}_S$ obtained in Section 3.2. Figure 3 shows the most adequate and inadequate models for the chair dataset: unsurprisingly, sofas and armchairs, which admit blocky cubifictions, are the most adequate models; while chairs with many intricate details are the least. Because our descriptor, and the subsequent similarity metric, are blind to these errors, removing these inadequate shapes from the graph shape space prevents them from appearing in shape morphings.

Similarity Metric

Using the cross structuring element, real-valued dilation allows to add a one-voxel margin to a shape. Thus, the added voxels all correspond to cells whose

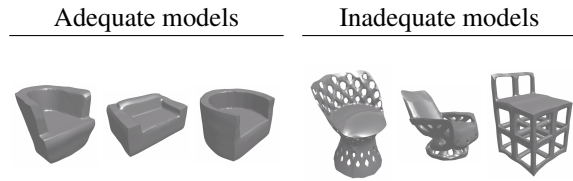| Adequate models	Inadequate models

Figure 3: Examples of adequate and inadequate models, with respect to our volumetric descriptor which averages density of presence within $8 \times 8 \times 8$ DVG cells.

L_1 distance to the shape is $1/r$. We can define a forward similarity metric D^{AB} from descriptor A to B, which penalizes the mass of B located outside the dilation of A:

$$D^{AB} = \min(\text{dilation}(A) - B, 0)$$
$$D^{BA} = \min(\text{dilation}(B) - A, 0) \quad (3)$$
$$d(A, B) \triangleq \|D^{AB}\|_1 + \|D^{BA}\|_1$$

Note that for all locations outside of dilation(A), the penalty imposed by $\|D^{AB}\|_1$ is the same as the L_1 voxel distance. Thus, for dissimilar models (e.g., if B is mostly located outside of dilation(A)), this metric d becomes less interpretable, because of the curse of dimensionality. We use this metric to build a shape graph $\mathcal{G}$, after all pairwise distances are evaluated. In general, each shape is connected to its k-nearest neighbors. However, the linking rules can vary for several reasons:

- Certain shapes may be particularly different from the rest of the dataset. In order to prevent them from being considered in morphings, we trim off links whose weights are above a threshold τ_w.

- To ensure that the final graph $\mathcal{G}$ is made of only one connected component, we can also decide to keep at least $k_{\min}$ connections for every node, even if their weights are above τ_w.

The impact of such trade-offs is discussed in Section 6.3.

4.3 Continuous Morphings

To find a minimal path in $\mathcal{G}$, we use Dijkstra's algorithm. The returned length corresponds to the energy of the minimal morphing, while the sequence of nodes provides a discrete morphing. Thanks to our invertible cubifiction, this shape sequence can be prolonged to a continuous morphing, by interpolating separately the style and content (V, C) of each shape. For the control points positions V, the interpolation is trivial and can just be linear; as for the interpolation of content values, we also propose linear interpolation. More precisely, we interpolate the cubified SDFs, and generate the geometry with marching cubes.

Because each edge in the path has a known length, the continuous path can be parameterized by arc length (see Discussion 6.6). For an arbitrary number of frames, whose positions are equally spaced along the path, this grants more interpolation frames in between less similar shapes, which are the most likely to have topology changes.

For a given sequence of style-content separated shapes $((V_1, C_1), ..., (V_k, C_k))$, and their corresponding edge lengths $L = (l_1^2, ..., l_{k-1}^k)$ in $\mathcal{G}$, we can formalize the continuous morphing using a time parameter $t \in [0,1]$:

$$
\begin{aligned}
i, i+1, \tilde{t} &= s_L(t) \\
\tilde{V} &= (1-t) \cdot V_1 + t \cdot V_k \\
y(t) &= p_{\text{tps}}^{\tilde{V}}((1-\tilde{t}) \cdot C_i + \tilde{t} \cdot C_{i+1})
\end{aligned}
\tag{4}
$$

Where $s_L(t)$ is the discrete arc lenth parameterization function, returning the indices $(i, i+1)$ of the edge nodes and the local time parameter $\tilde{t}$. Note that the interpolation on V is straight from V_1 to V_k: the graph $\mathcal{G}$ is only used for interpolating the content C.

The same framework can be used to morph between new, unknown shapes, by embedding them into graph $\mathcal{G}$, following all the steps: DVG optimization, shape cubifiction, links creation to connect these new shapes to the already-existing graph.

5 RESULTS

We conducted our experiments using shapes from the ShapeNet (Chang et al., 2015) dataset; more specifically using 500 from the chair category and 200 from the car category. Because the continuous morphings require all shapes to be closed manifolds, and for fair comparisons against (Kleineberg et al., 2020) which preprocesses shapes the same way, we first converted them into manifolds using the same method as (Park et al., 2019). We then sampled $l = 4096$ points to be used as the DVG input pointclouds.

5.1 Shape Morphings

To produce shape morphings, we randomly picked pairs of nodes in $\mathcal{G}$, and applied the method explained in Section 4.3. Following Equation (4), each morphing consists in a sequence of triplets $(\tilde{V}, \tilde{C}, y)$. While we are typically only interested in the final geometry y, observing $\tilde{V}$ and $\tilde{C}$ provides, along with the found minimal path in $\mathcal{G}$, an explanation for the generated geometries. We show such triplets in Figure 5.

5.2 Robustness to Misalignment

We assume all our shapes are consistently aligned, as standard among generative models. However, being a deformable model, we tested the ability of the DVG to converge to the correct configuration when the input shape has been rotated. Given the hierarchical subdivisions and the centrality of the first levels (see discussion in Section 6), we compared the determined first level for two conditions: ground truth alignment, and noisy alignment (rotation with random Euler angles, according to $\mathcal{N}(0, \sigma = 0.2\text{rad} \approx 12°)$). For fairness, we kept a constant number of gradient descent steps. The error is then measured as the Euclidean distance between the control points of the two grids, $\|\text{GT} - \text{pred}\|_2$. Figure 6 shows an example of a misaligned grid

We also estimated, for any given τ_θ, $\mathbb{E}_{\theta_{\max} \leq \tau_\theta}(\|\text{GT} - \text{pred}\|_2)$, the empirical expectancy on datasets where the maximum angular error is smaller than a threshold τ_θ (see plot in Figure 6). We observe that it increases at a reasonably low pace, confirming the advantages of a deformable model. As for high angular errors (more than $30°$), the predicted grid can be flipped: a control point which should be at the top is now located on the side. For a single shape, this is not a problem. However, on a whole dataset, this would break the consistent cubifiction we require to build our similarity measure.

5.3 Qualitative Analysis: Comparison with Deep Learning

In our work, one of the main objectives was to produce results comparable in quality to those obtained via deep learning. We chose to compare our results to the adversarial neural network developed by (Kleineberg et al., 2020), as it also relies on an SDF representation, and has published the weights of a pre-trained network, allowing us to produce new morphings.

For fair comparisons, we adopted the following methodology:

- We kept our graph $\mathcal{G}$ untouched, built from the same 500 chair examples as in the previous experiments;

- We first generated baseline morphings as latent space interpolations between random codes corresponding to chairs (about 4k examples);

- For each of these morphings, we extracted the first and last states: these provided query shapes that we embedded in $\mathcal{G}$ (as explained in Section 4.3) in order to generate our morphings;
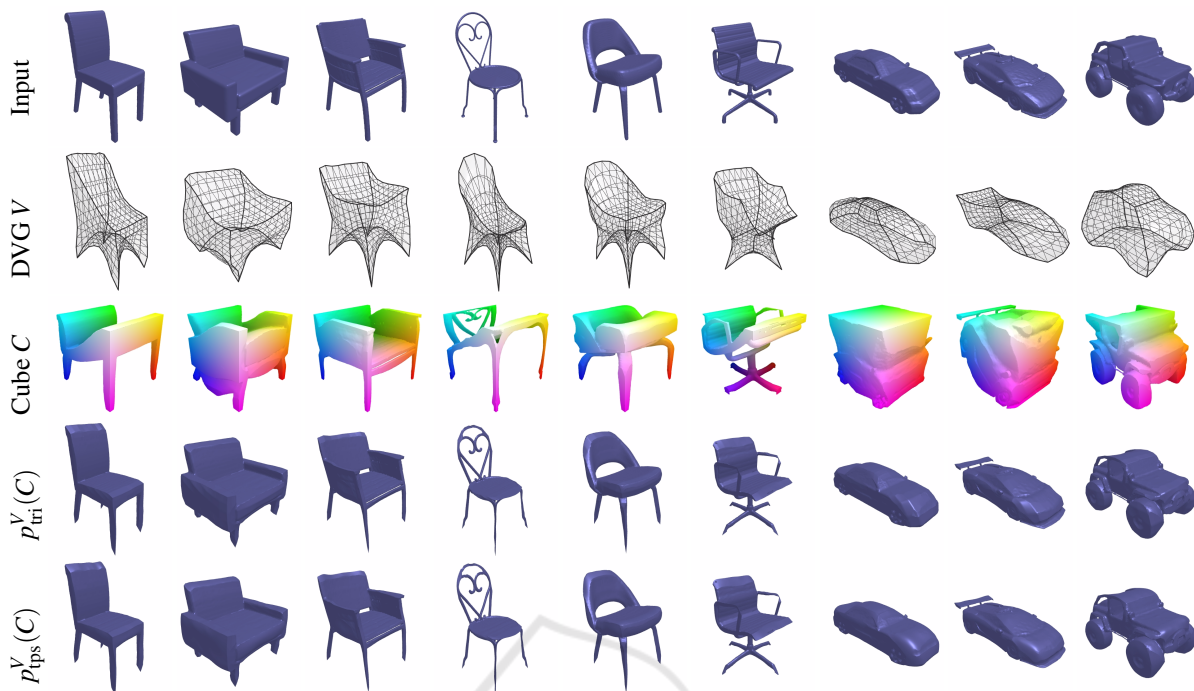
Figure 4: (Zoom in to see details) Qualitative results for shape reconstruction via DVGs: estimating V for each shape allows to cubify it (C), and this can be reprojected into V by a trilinear p_{tri}^V or a spline p_{tps}^V projector (see 3.1), the latter yielding smoother surfaces. The cubified shapes are color-coded by assigning a value in $[0,1]^3$ to an RGB color.

- To match the surface quality of (Kleineberg et al., 2020), we decreased the resolution of our SDFs before the mesh reconstruction via marching cubes.

Figure 7 presents some comparative results, selected for their representativity. Here are our observations for each of the five shown examples:

1. These shapes happened to have a direct link when embedded in $\mathcal{G}$: the morphing entirely comes from the DVG.

2. While the morphing of the seat is visually pleasing, the SDF interpolation is responsible for a hole in the leg (frames 4–10).

3. The armrests removal looks less pleasing, but on the flip side, the progressive rounding of the back is more natural.

4. Most of the artifacts (frames 7–12) come from the short-circuit effect, discussed in 6.5.

5. Apart from similar surface artifacts, it exemplifies the impact of our minimal paths for chair-to-armchair morphings. Indeed, they appear to favor transitions which add thin armrests halfway through.

When watched as videos, our morphings also appear generally less smooth. This is due to our SDF interpolations: when new mass appears within the 1-voxel margin, it can look sudden, and then less pleasant

to the eye. Despite these imperfections, we found it pretty remarkable to achieve such results while only relying on a much smaller dataset. It would indeed seem hard, if not impossible, to train a neural network with such limited data.

6 DISCUSSION

Our overall method comprises many components, each requiring design choices which influence the quality of the results. Because the systematic analysis of general shape morphing (for non-parametric shapes) is still uncharted territory, we presented quantitative and qualitative results where each component is designed in the minimally-viable way. However, our system admits many local improvements.

Hence the following observations and suggestions, noted from our experiments.

6.1 Importance of the First Hierarchical Levels

While (Groscot and Cohen, 2022) establishes the importance of the progressive refinement of DVGs, our experiments further emphasize the greater importance of the first levels. If the second level is unfrozen before
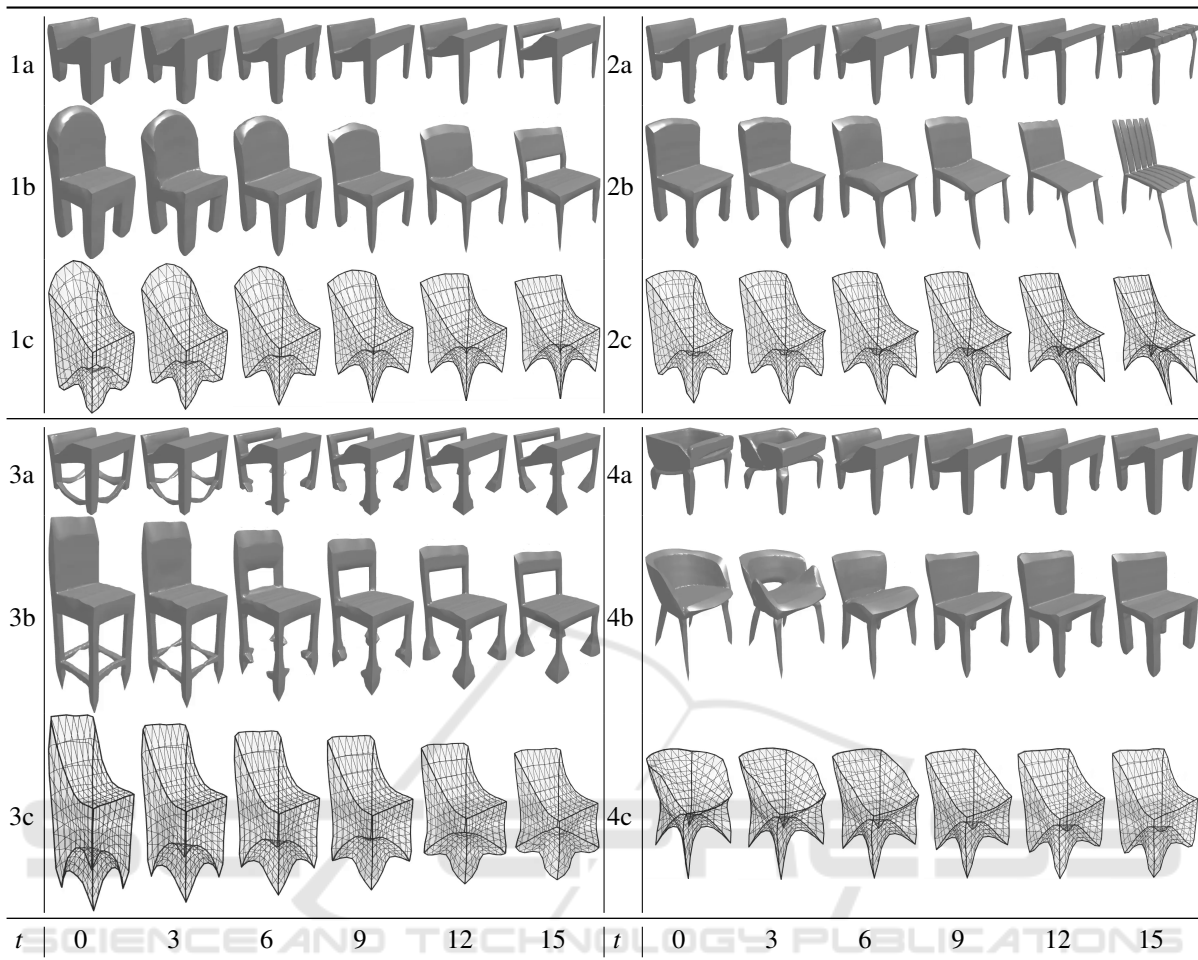
Figure 5: (Zoom in to see details) Examples of morphings generated with our method. Rows (*a*), (*b*), and (*c*) respectively correspond to the interpolation of cubes *C*, final shapes, and DVG grids *V*.

the first level has correctly converged, the misalignment of the cube edge with the dominant features of the shape will remain. This problem can arise when optimizing a batch of DVGs on many shapes, with a constant number of epochs per level. To prevent this from happening, one has to make sure the first level has enough time to converge on all the training shapes, or resort to an adaptive gradient descent scheme.
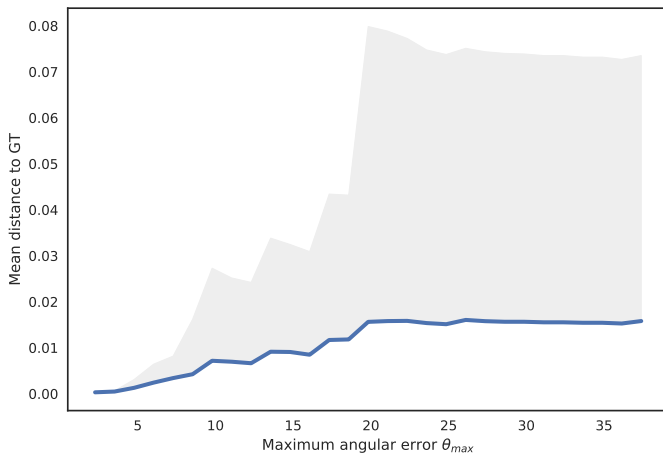
6.2 Manual Edition of a DVG

In a real use case scenario, a determined DVG can be manually corrected. For instance, it can easily be symmetrized – by averaging with its symmetric. This could be useful for shape reconstructions and morphings, to ensure that the generated geometries are indeed symmetric. All the results we show did not resort to any manual correction, in order to exhibit the bare abilities of our model. Yet it would be interesting,

for future work, to investigate the usefulness of ad-hoc post-processing.

6.3 Graph Connectivity

The quality of the morphings generated by our method depends on the graph building procedure, and more specifically, the node linking rule. Ordinarily, these graphs can be built obeying either a k-nearest neighbor condition, or a distance threshold condition. By design, our metric becomes less interpretable as the estimated distance increases. This is why we need to impose a distance threshold criteria. Doing so, the graph can however have several connected components, limiting the ability to interpolate between shapes of distinct modes (say, between an office chair and a sofa).

In practice, finding threshold values can be hard, given the non-uniform distribution of pairwise distances (for instance, we observed that the distances

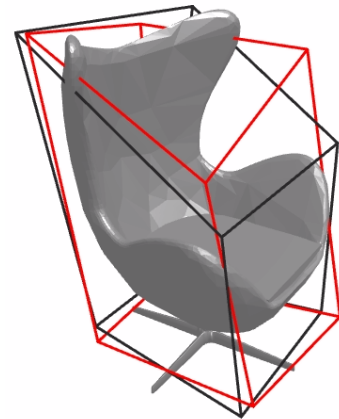(a) Prediction error against shape misalignment

(b) Misaligned v_0

Figure 6: (a) Mean error against maximum rotation angle θ_{max}, grey area is the standard deviation; (b) Ground truth in black, misaligned prediction in red, where $\theta_{max} \approx 20°$, error $= 0.078$. Refer to Section 5.2 for a discussion on these figures.

between many sofas are disproportionately small). To mitigate the potential mistakes, we build the k-nearest neighbor graph with three constraints, in decreasing priority: for node i,

1. $k_i \geq k_{min}$
2. $k_i \leq k_{max}$
3. $\forall j \leftrightarrow i, d(S_i, S_j) \leq \tau_w$

6.4 Volumetric Descriptor Sensitivity and Specificity

In order to preserve fine information in the volumetric descriptor, we decided to average the indicator function $\mathbb{1}_S$ within each DVG cell, instead of keeping all cells where it is non null (which would correspond to a classical voxelization). However, the values can be small, and have a negligible influence on the similarity measure, even where there is non-negligible mass. Take the example of a half cube within a DVG cell, its average presence density is $1/2^3 = 1/8 = 0.125$. This is why we propose to apply the cubic root as a contrast function to increase sensitivity to low values – before feeding the descriptors to the similarity metric $d(A, B)$.

We also performed experiments where the resolution of the volumetric descriptor is $r = 16$, effectively halving the one-voxel margin tolerance. With this increased specificity, neighbors are more similar than before; but dissimilar models are further away than before. This led to discrete morphings which all contain many intermediate steps. Overall, the generated morphings were unpleasantly convoluted. We then settled for $r = 8$ as it appeared to be the best compromise, on our chair dataset.

6.5 Misleadingly Low Similarity and Short Circuits

Models whose topology is not adequately represented by our metric are, as explained in Section 4.2, not included in the graph. More precisely, we exclude the 20% most inadequate models.

But some models, not excluded from previous considerations, can badly influence the quality of morphings: those which display sharp surface features, not captured by our descriptor. They are typically not amongst the most adequate models, but still passed the aforementioned 20% threshold. Such a situation is depicted in Figure 7, rows (a).

Another interesting phenomenon appears when a pair of unwanted models hijacks many morphings. If they are each connected to distinct regions of $\mathcal{G}$, they provide a short circuit to many minimal paths.

This is the case for models at locations (1a,11) and (1a,12). They indeed appeared in many of our randomly generated morphings, creating unwanted surface artifacts. We show, in rows (b), that manually discarding these undesired models and short circuits can enhance the quality of the outputs. However, we kept all the other morphings we show in this paper untouched, in order to exhibit the results without any manual intervention.

6.6 Metric and Arc-Length Parameterization

Because our similarity measure $d(A, B)$ only penalizes difference in shapes beyond a one-voxel margin, many pairs of shapes have a low distance, sometimes even
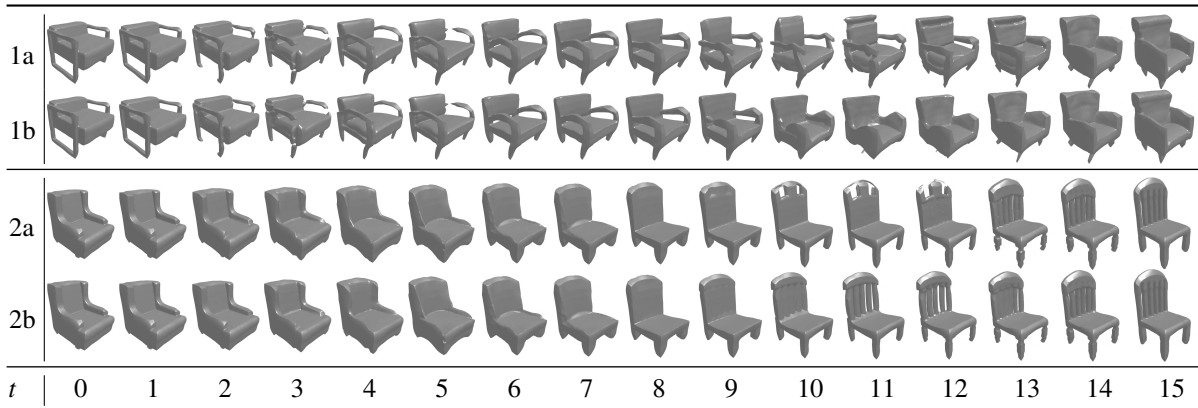
Figure 7: (Zoom in to see details) Manual intervention on morphings: some generated morphings can display unsightly intermediate shapes because of the found minimal path (see (a) rows, at times 10 through 12). Manually discarding the unwanted models from the graph allows to redetermine an alternative, more pleasing, morphing ((b) rows).

null. This is due to the fact that the dataset contains many redundant shapes, with similar content C (for instance, many chairs resembling the model on Figure 7 at (1a,0). Contrary to the previous discussion 6.5 (on misleadingly low similarity), this is the case where similarities ought to be low. Conversely, for dissimilar shapes, the edge length can be disproportionately large, accounting for most of the total path length.

Since the discrete paths make continuous morphings by arc-length parameterization, this issue can lead to unpleasing morphings. It could have ben addressed in two ways:

1. Regrouping, like (Gao et al., 2013), cliques of interconnected shapes; and allowing at most one representative of a clique within a morphing;

2. Applying a non-linear transformation on the path length, before the generation of the continuous morphing.

We opted for the second option as it is the simplest and provides the baseline we are aiming for. We apply the function $x \mapsto 1 + \sqrt{x}$, where the square root rebalances low and high values, and the constant 1 corrects for the almost-null edge lengths.

7 CONCLUSION

The idea presented in this paper is, essentially, to connect shapes similar in content, so that morphing between them is "simple": the DVG cubifiction trick makes such a simple formulation of morphings possible. As we have shown, performing a simple linear interpolation on cubified SDFs already generates qualitatively pleasing morphings, therefore establishing a strong baseline. More complex approaches, based for instance on optimal-transport, could probably yield

better results. Yet, we produced results qualitatively similar to the state-of-the-art deep learning methods, while relying on limited data.

Even if our DVG shape parameterization is not specific to any class, we restricted our analysis to chairs, because of the challenges posed by their varied topologies, and also showed initial results on cars. Moreover, their strong reflection symmetries are compatible with cubifiction.

For future work, we would like to investigate the use of this model on shape categories displaying less symmetries. It would also be interesting to reproduce these results at a larger scale, say with the complete chair subset of ShapeNet, or even when adding other categories to the same graph: would we find different shape types separated in different clusters?

Finally, we could bridge the gap between our method and neural networks. Indeed, the SDFs interpolations are inherently limited and may not be able to fully capture shape priors, even in a large scale application. In this case, a generative model, trained only on cubified shapes for instance, could provide an interesting solution.

ACKNOWLEDGEMENTS

REFERENCES

Achlioptas, P., Diamanti, O., Mitliagkas, I., and Guibas, L. J. (2017). Learning representations and generative models for 3D point clouds.

Allen, B., Curless, B., Curless, B., and Popović, Z. (2003). The space of human body shapes: Reconstruction and parameterization from range scans. *ACM Trans. Graph.*, 22(3):587–594.

Barreira, N., Penedo, M. G., Mariño, C., and Ansia, F. M. (2003). Topological active volumes. In Petkov, N. and Westenberg, M. A., editors, *Computer Analysis of Images and Patterns*, pages 337–344, Berlin, Heidelberg. Springer Berlin Heidelberg.

Chang, A. X., Funkhouser, T., Guibas, L., Hanrahan, P., Huang, Q., Li, Z., Savarese, S., Savva, M., Song, S., Su, H., Xiao, J., Yi, L., and Yu, F. (2015). ShapeNet: An Information-Rich 3D Model Repository. Technical Report arXiv:1512.03012 [cs.GR], Stanford University — Princeton University — Toyota Technological Institute at Chicago.

Cohen, L. D. (1991). On active contour models and balloons. *CVGIP: Image Understanding*, 53(2):211 – 218.

Dubrovina, A., Xia, F., Achlioptas, P., Shalah, M., Groscot, R., and Guibas, L. J. (2019). Composite shape modeling via latent space factorization. In *The IEEE International Conference on Computer Vision (ICCV)*.

Fan, H., Su, H., and Guibas, L. J. (2016). A point set generation network for 3D object reconstruction from a single image. *CoRR*, abs/1612.00603.

Fish, N., Averkiou, M., van Kaick, O., Sorkine-Hornung, O., Cohen-Or, D., and Mitra, N. J. (2014). Meta-representation of shape families. *ACM Trans. Graph.*, 33(4):34:1–34:11.

Gao, L., Lai, Y.-K., Huang, Q., and Hu, S. (2013). A data-driven approach to realistic shape morphing. *Computer Graphics Forum*, 32.

Goodfellow, I. J., Pouget-Abadie, J., Mirza, M., Xu, B., Warde-Farley, D., Ozair, S., Courville, A., and Bengio, Y. (2014). Generative adversarial networks.

Groscot, R. (2021). *Separable 3D Shape Representations for Shape Processing*. PhD thesis. Thèse de doctorat dirigée par Cohen, Laurent David Mathématiques appliquées Université Paris sciences et lettres 2021.

Groscot, R., Cohen, L., and Guibas, L. (2019). Shape part transfer via semantic latent space factorization. In Nielsen, F. and Barbaresco, F., editors, *Geometric Science of Information*, pages 511–519, Cham. Springer International Publishing.

Groscot, R. and Cohen, L. D. (2022). Deformable voxel grids for shape comparisons. In Jiang, X., Tao, W., Zeng, D., and Xie, Y., editors, *Fourteenth International Conference on Digital Image Processing (ICDIP 2022)*, volume 12342, page 123423G. International Society for Optics and Photonics, SPIE.

Groueix, T., Fisher, M., Kim, V. G., Russell, B., and Aubry, M. (2018). AtlasNet: A Papier-Mâché Approach to Learning 3D Surface Generation. In *CVPR 2018*, Salt Lake City, United States.

Haibin, H., Kalogerakis, E., and Marlin, B. (2015). Analysis and synthesis of 3D shape families via deep-learned generative models of surfaces. *Computer Graphics Forum*, 34.

Hanocka, R., Fish, N., Wang, Z., Giryes, R., Fleishman, S., and Cohen-Or, D. (2018). Alignet: Partial-shape agnostic alignment via unsupervised learning.

Hao, Z., Averbuch-Elor, H., Snavely, N., and Belongie, S. (2020). Dualsdf: Semantic shape manipulation using a two-level representation. In *Proceedings of the IEEE/CVF Conference on Computer Vision and Pattern Recognition (CVPR)*.

Hemalatha, R., Thamizhvani, T., Dhivya, A. J. A., Joseph, J. E., Babu, B., and Chandrasekaran, R. (2018). Active contour based segmentation techniques for medical image analysis. In Koprowski, R., editor, *Medical and Biological Image Analysis*, chapter 2. IntechOpen, Rijeka.

Kalogerakis, E., Chaudhuri, S., Koller, D., and Koltun, V. (2012). A probabilistic model for component-based shape synthesis. *ACM Trans. Graph.*, 31(4):55:1–55:11.

Kass, M., Witkin, A., and Terzopoulos, D. (1988). Snakes: Active contour models. *International Journal of Computer Vision*, 1(4):321–331.

Kingma, D. P. and Welling, M. (2013). Auto-Encoding Variational Bayes. *arXiv e-prints*, page arXiv:1312.6114.

Kleineberg, M., Fey, M., and Weichert, F. (2020). Adversarial generation of continuous implicit shape representations.

Kurenkov, A., Ji, J., Garg, A., Mehta, V., Gwak, J., Choy, C., and Savarese, S. (2017). Deformnet: Free-form deformation network for 3d shape reconstruction from a single image.

Li, J., Xu, K., Chaudhuri, S., Yumer, E., Zhang, H., and Guibas, L. J. (2017). GRASS: Generative recursive autoencoders for shape structures. *ACM Transactions on Graphics (Proceedings of SIGGRAPH 2017)*.

Lorensen, W. E. and Cline, H. E. (1987). Marching cubes: A high resolution 3d surface construction algorithm. SIGGRAPH '87, New York, NY, USA.

Niemeyer, M., Mescheder, L., Oechsle, M., and Geiger, A. (2019). Occupancy flow: 4d reconstruction by learning particle dynamics. In *International Conference on Computer Vision*.

Park, E., Yang, J., Yumer, E., Ceylan, D., and Berg, A. C. (2017). Transformation-grounded image generation network for novel 3d view synthesis. In *Proceedings of the IEEE Conference on Computer Vision and Pattern Recognition (CVPR)*.

Park, J. J., Florence, P., Straub, J., Newcombe, R., and Lovegrove, S. (2019). Deepsdf: Learning continuous signed distance functions for shape representation. In *Proceedings of the IEEE/CVF Conference on Computer Vision and Pattern Recognition (CVPR)*.

Qi, C. R., Su, H., Mo, K., and Guibas, L. J. (2016). Pointnet: Deep learning on point sets for 3D classification and segmentation.

Qi, C. R., Yi, L., Su, H., and Guibas, L. J. (2017). Pointnet++:

Deep hierarchical feature learning on point sets in a metric space. *CoRR*, abs/1706.02413.

Sederberg, T. W. and Parry, S. R. (1986). Free-form deformation of solid geometric models. *SIGGRAPH Comput. Graph.*, 20(4):151–160.

Shin, D., Fowlkes, C. C., and Hoiem, D. (2018). Pixels, voxels, and views: A study of shape representations for single view 3d object shape prediction. In *2018 IEEE/CVF Conference on Computer Vision and Pattern Recognition*, pages 3061–3069.

Tatarchenko, M., Dosovitskiy, A., and Brox, T. (2017). Octree generating networks: Efficient convolutional architectures for high-resolution 3D outputs. *CoRR*, abs/1703.09438.

Tulsiani, S., Su, H., Guibas, L. J., Efros, A. A., and Malik, J. (2017). Learning shape abstractions by assembling volumetric primitives. In *Computer Vision and Pattern Regognition (CVPR)*.

Wang, N., Zhang, Y., Li, Z., Fu, Y., Liu, W., and Jiang, Y.-G. (2018). Pixel2mesh: Generating 3d mesh models from single rgb images. In *ECCV*.

Wu, J., Zhang, C., Xue, T., Freeman, W. T., and Tenenbaum, J. B. (2016). Learning a probabilistic latent space of object shapes via 3D generative-adversarial modeling. In *Proceedings of the 30th International Conference on Neural Information Processing Systems*, NIPS'16, pages 82–90, USA. Curran Associates Inc.

Zheng, Z., Yu, T., Dai, Q., and Liu, Y. (2020). Deep implicit templates for 3d shape representation.